analytical chemistry

Article

Cite This: *Anal. Chem.* 2019, 91, 6127−6133

pubs.acs.org/ac

Programming a Target-Initiated Bifunctional DNAzyme Nanodevice for Sensitive Ratiometric Electrochemical Biosensing

Yunrui Li, Yuanyuan Chang, Jing Ma, Zhongyu Wu, Ruo Yuan,* and Yaqin Chai*

Key Laboratory of Luminescent and Real-Time Analytical Chemistry (Southwest University), Ministry of Education, College of Chemistry and Chemical Engineering, Southwest University, Chongqing 400715, People's Republic of China

Supporting Information

ABSTRACT: Here, a bifunctional DNAzyme nanodevice (BFDN) with two detection paths toward the same target was intelligently designed and applied to construct a ratiometric electrochemical biosensor for highly reliable and sensitive mercury ion (Hg^{2+}) detection. In the presence of the target Hg^{2+}, the T-Hg^{2+}-T pair could actuate the preassembled DNA four-branched nanostructure (DNA-4B) without cleavage capability transform to the BFDN with strong cleavage capability for triggering two synchronous Hg^{2+} detection paths, including a "signal-off" path (**1**) that consisted of a cascade DNAzyme cleavage reaction to dramatically decrease the ferrocene (Fc) response and a "signal-on" path (**2**) that accomplished the capture of significant amounts of methylene blue (MB) on the electrode surface under the assistant of DNAzyme2 (D2) in BFDN. This strategy not only effectively avoided the false positive signal compared with traditional single paths, but also proposed a new ratiometric method to successfully circumvent the deficiency that existed in previous ratiometric electrochemical biosensors. As a result, the reliable and sensitive Hg^{2+} detection was achieved in the range from 0.1 pM to 200 nM with a detection limit of 23 fM. Above all, here, the assembly of the BFDN is ingeniously coupled with amplification strategy, paving a promising avenue to promote the performances of simple multifunctional DNA nanomachines and facilitate the corresponding development of DNA nanomachines in biosensor platform.

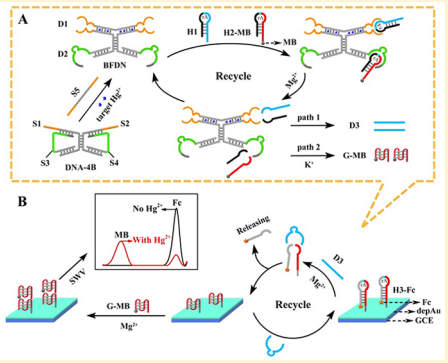

The electrochemical ratiometric method, combining "signal-on" and "signal-off" strategies, has been proven wonderful, because of its obvious advantages, including self-referencing capability, high reliability and accuracy, good reproducibility, low detection limit, wide linear range and so on, which inspires researchers constructed a series labeled ratiometric electrochemical biosensors for analysis and detection.[1] For example, Wu et al. achieved Aflatoxin B1 detection with ratiometric electrochemical assay.[2] Xiong also proposed an electrochemical ratiometric method for ultrasensitive nucleic acids detection with enzyme-assisted target recycling amplification strategy.[3] In those labeled ratiometric electrochemical biosensors, the targets simultaneously induce two types of signal changes, where one is performed through capturing or releasing of redox label and another is achieved by altering the distance between redox label and electrode surface, providing a built-in correction toward signal transduction and overcoming target-independent interferences that are difficult to avoid in single-signal detection patterns.[4−6] However, the distance-dependent signal adjustment strategy here is often far from the most ideal way that may negatively disturbs the performance of ratiometric electrochemical biosensors for following reasons: (1) Inconsistent results are reported that whether the redox label located on the proximal end of the surface-bound DNA can get greater currents compared with the distal end, because of the fluctuation of complex nature of DNA interfaces, disturbing the well cognition about how the position of the redox label impacts the electron transfer between the redox label and electrode surface.[7] (2) Many current studies have demonstrated that different redox labels have different sensitivity to distance, such as Fc exhibits highly sensitive to its position on DNA duplexes, while MB is not.[8−11] Therefore, the selection of redox label when designing biosensors is not arbitrary but a non-negligible part that must be given attention, which undoubtedly increases the design burden. (3) Accurate distance adjustment on the electrode surface cannot be achieved. Not all probes tethered to electrodes are in an ideal upright state, DNA local disorder including DNA entanglement, tilting, elastic bending, rotational motions, and nonspecific interactions may interfere with the expected distance change between redox label and electrode surface, further affecting biosensors performance.[12,13] In addition, it is found that dual-signal sensing in those ratiometric electrochemical biosensors is implemented with single detection path.[14−16] Notwithstanding considerable superiority in its simplicity, the single detection path lacks self-monitoring toward entire experimental process, greatly limiting the promotion of reliability. Hence, based on above analysis, it is of critical importance to circumvent these

Received: February 6, 2019
Accepted: April 1, 2019
Published: April 1, 2019

DOI: 10.1021/acs.analchem.9b00690
Anal. Chem. 2019, 91, 6127−6133

Scheme 1. Schematic Illustration of the Proposed Ratiometric Electrochemical Biosensor: (A) The Assembly of Hg^{2+}-Initiated BFDN and Efficient DNAzyme Amplification Progress and (B) Electrode Modification and Signal Output Process

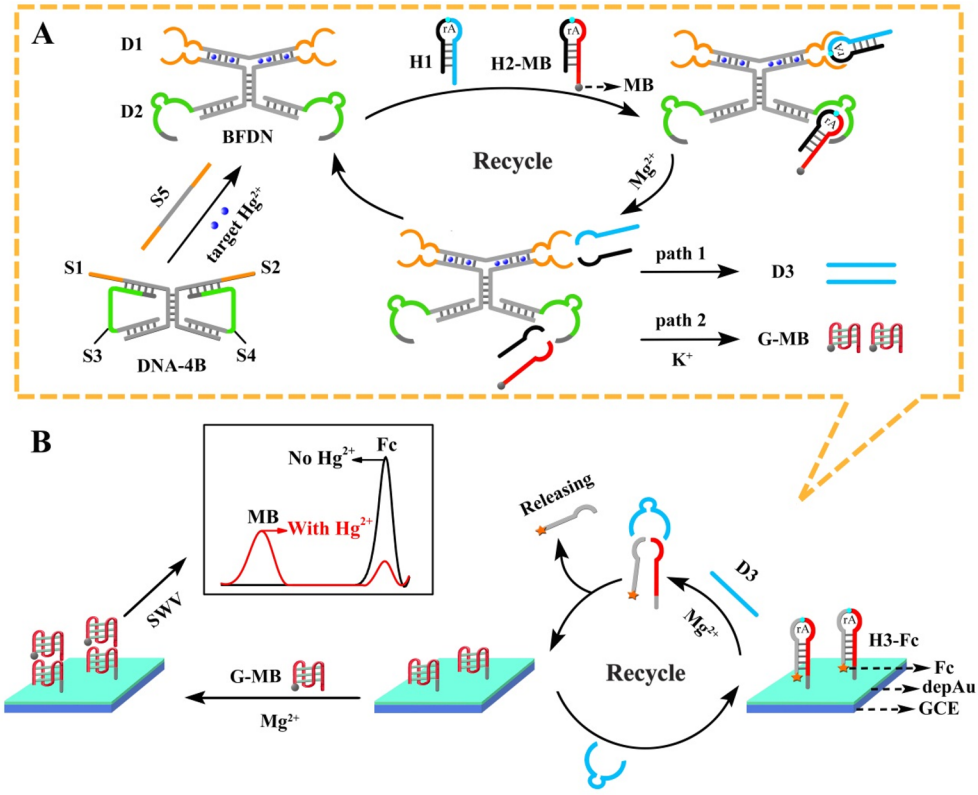

mentioned deficiencies derived from distance-dependent signal adjustment strategy and single detection path, constructing new ratiometric electrochemical biosensors with well performances.

DNA nanoscience,[17] as an indispensable technology for building new biosensor platform, has proposed many intriguing DNA nanostructures and exquisite DNA nanodevices such as hairpin DNA,[18] DNA nippers,[19] DNA tetrahedron,[20,21] and DNA walker.[22] They are extensively used and often perform a specific function, for instance, hairpin DNA tethered to electrode is served as capture probe and DNA tetrahedron play a role in improving the capture efficiency.[23,24] While, of course, multifunctional structures have also become increasingly popular recently.[25] For example, based on three types of Y-shaped functional DNA domains and a DNA connector, Wu et al. built a multifunctional DNA nanodevice for cancer therapy.[26] However, it is obvious that the complexity of such multifunctional DNA nanodevice is actually a daunting obstacle, requiring not only multiple DNA strands, but also intricate operation, severely hindering their further development in biosensing system. Fortunately, branched DNA nanostructures effectively overcame the complexity challenge, because of inherent advantages of being able to precisely place different molecules in close proximity,[27−30] facilitating the flourish of simple multifunctional DNA nanodevices. Nevertheless, these multifunctional DNA nanodevices are still subject to another serious defect: current assembly of multifunctional DNA nanodevices focuses more on the development of theirs diverse identification functions, while neglecting to combine with mature signal amplification strategies which usually employ protein enzymes, catalytic nanoparticles, catalytic nucleic acid (DNAzyme), or target recycling technique as tools.[31−35] Thereinto, the properties of good stability, easy preparation, and low nonspecific adsorption have turned the DNAzyme into ideal candidate.[36,37] Thus, to integrate multifunctional DNA nanodevices with DNAzyme amplification strategy would be highly desirable in such situation, which may be very promising to improve the performances of multifunctional DNA nanodevices.

To our surprise, it was found that the application of multifunctional DNA nanodevices to ratiometric electrochemical biosensors could simultaneously activate multiple detection paths toward the same target and also successfully conquer the defect of distance-dependent signal adjustment strategy existed in the previous ratiometric method, realizing highly reliable and sensitive target detection. Hence, a simple Hg^{2+}-initiated bifunctional DNAzyme nanodevice (BFDN) emerged in this work to build a novel ratiometric electrochemical biosensor with high performance for sensitive Hg^{2+} detection. The relative design principle and construction process of this biosensor were illustrated in Scheme 1. First, we assembled a DNA four-branched nanostructure (DNA-4B) using four types of DNA strands (S1, S2, S3, and S4), in which the yellow parts represented split Mg^{2+}-dependent DNAzyme1 (D1) subunits and the green parts were locked-Mg^{2+}-dependent DNAzyme2 (D2) sequence. In the presence of Hg^{2+}, the S1 and S2 in DNA-4B could be cointeractive with S5 containing split D1 subunits via T-Hg^{2+}-T coordination chemistry, triggering DNA-4B without cleavage capability converted into BFDN with strong cleavage capability. A BFDN possessed four functional domains comprised by two D1 and two D2, which actuated two detection paths simutaneously: path 1 and path 2.

DOI: 10.1021/acs.analchem.9b00690
Anal. Chem. 2019, 91, 6127−6133

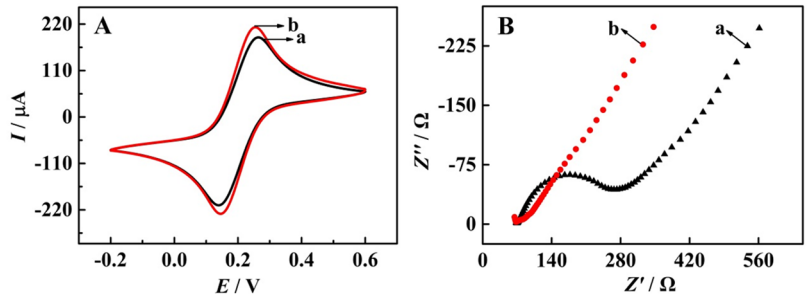

Figure 1. (A) CV and (B) EIS characterizations of the modified electrode at different stages in 5 mM $[Fe(CN)_6]^{3-/4-}$ solution: (a) bare GCE and (b) depAu/GCE.

In path 1, with the assistant of Mg^{2+}, D1 could recognize H1 and then cleave at ribonucleobase (rA) site, yielding DNAzyme3 (D3) that further cleaved H3-Fc immobilized on the electrode surface, releasing an abundance of ferrocene (Fc) to dramatically decrease the Fc signal response and leaving many G-rich fragments to fold into G-quadruplexes on the electrode surface after multiple recycling cleavages. In path 2, likewise, D2 in BFDN also could continuously cleave H2-MB (labeled with Methylene Blue at the 3′-terminal) in the presence of Mg^{2+} to output a large number of G-rich sequences labeled with MB. Then these sequences folded into MB-labeled G-quadruplexes (G-MB) and spontaneously self-assembled with the MB-free G-quadruplexs remained on the electrode surface by $\pi-\pi$ stacking, leading to efficient capture of G-MB with high MB response signal. By virtue of such design, here, path 1 and path 2 not only could be cross-referenced to efficiently monitor entire experimental process, but also accomplished the "off−on" configuration, achieving highly reliable and sensitive Hg^{2+} detection with a ratiometric method. In addition, note that the proposal of BFDN in this work paves a promising avenue to assemble more powerful multifunctional DNA nanomachines by integrating amplification strategies, further promoting the development of DNA nanomachines in biosensor platform.

EXPERIMENTAL SECTION

Assembly of the Bifunctional DNAzyme Nanodevice (BFDN). In short, DNA single strands S1, S2, S3, and S4 (1 μM) with equal volume (10 μL) were first mixed together, followed by further heating to 95 °C for 5 min and quickly cooling to 4 °C within 30 s for assembling DNA-4B. Subsequently, with the introduction of 10 μL S5 (1 μM) and 10 μL different concentrations target Hg^{2+} for 2 h, Hg^{2+}-mediated T-Hg^{2+}-T pair could activate the interaction between DNA-4B and S5, successfully converting DNA-4B into BFDN.

Cleavage Amplification of the Bifunctional DNAzyme Nanodevice (BFDN). The BFDN containing four functional domains (two D1 and two D2) could circularly cleave H1 and H2 labeled with MB (H2-MB), respectively under the help of Mg^{2+}. In detail, 60 μL BFDN was mixed with 10 μL H1 (2 μM) and 10 μL H2-MB (2 μM) for 60 min at 37 °C. During the period, D1 in BFDN selectively recognized substrate H1 and then cleaved at ribonucleobase (rA) site, obtaining numerous D3 segments after multiple cycles. With the same way, the D2 also could undergo many cycles to continuously cleave H2-MB, releasing plenty of G-rich sequences that folded into G-quadruplexes (G-MB). Therefore, by virtue of BFDN, H1 and H2-MB were tactfully converted into corresponding D3 and G-MB, significantly enhancing the sensitivity of target Hg^{2+} detection.

Fabrication of the Proposed Ratiometric Electrochemical Biosensor. Prior to surface modification, glassy carbon electrode (GCE) was carefully polished with alumina slurry and sonicated. The cleaned GCE was then immersed in $HAuCl_4$ solution (1%) and electrodeposited to obtain gold particles (depAu). Next, H3-Fc (2 μM, 10 μL) was dropped on electrode and incubated overnight. The modified electrode was finally incubated with 10 μL the cleavage products of BFDN (D3 and G-MB) for 80 min at 37 °C. After cleaning, the finished electrode could be used for measurements.

Electrochemical Measurements. The CV and EIS electrochemical measurements were conducted in 5 mM $[Fe(CN)_6]^{3-/4-}$ solution. CV signal was measured in potential ranging from −0.2 to 0.6 V. EIS was recorded in the ac frequency ranging from 10^{-1} to 10^5 Hz with an excitation signal of 5 mV and formal potential of 220 mV. The SWV response was obtained in PBS solution (pH 7.0) with potential range of −0.6 to 0.8 V (vs saturated calomel electrode), which was used to assess the performance of this ratiometric electrochemical biosensor.

RESULTS AND DISCUSSION

Stepwise Characterization of the Modified Electrode. CV and EIS were conducted to characterize the modification of the electrode, respectively. In Figure 1A (CV), first, typical redox peaks of $[Fe(CN)_6]^{3-/4-}$ (curve a) were gained for the bare GCE. Then, once gold particles (depAu) were introduced onto the bare GCE, the peak current increased (curve b), attributing to the fact that the pre-eminent conductivity of depAu was able to efficiently speed up electron transfer. These characterizations clearly revealed that the preparation of the electrode was successfully.

Figure 1B (EIS) was the impedance spectra of the modified electrode. Compared with the bare GCE (curve a), the value of electron-transfer resistance (R_{et}) of depAu/GCE (curve b) significantly decreased, implying the good conductivity of depAu. These results were consistent with that observed in CV, proving the successful preparation of the electrode once again.

Feasibility of the Ratiometric Electrochemical Biosensor. To confirm the feasibility of the ratiometric electrochemical biosensor, the SWV measurements were performed on different modified electrodes in PBS solution. As shown in Figure 2, only an obvious oxidation peak of Fc at ~0.49 V (curve a) was recorded when the depAu/GCE was modified with H3-Fc. Then, the response of H3-Fc/depAu/GCE toward 0 nM Hg^{2+} was also observed (curve b), which

DOI: 10.1021/acs.analchem.9b00690
Anal. Chem. 2019, 91, 6127−6133

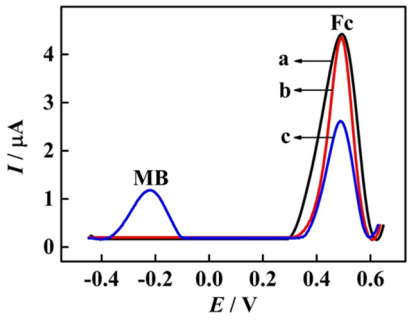

Figure 2. SWV responses of H3-Fc/depAu/GCE (curve a, black) and H3-Fc/depAu/GCE after treating with the cleavage products (D3 and G-MB) of different concentrations Hg^{2+}-initiated BFDN (0 nM Hg^{2+} (curve b, red) and 0.1 nM Hg^{2+} (curve c, blue).

almost the same as that of curve a, because of the fact that 0 nM Hg^{2+} could not initiate the assembly of BFDN, lacking cleavage products (D3 and G-MB) to react with H3-Fc/depAu/GCE. However, once a small amount of Hg^{2+} was introduced, many cleavage products (D3 and G-MB) of Hg^{2+}-initiated BFDN could be obtained to further react with H3-Fc/depAu/GCE, resulting the oxidation peak of Fc significantly decreased and a new oxidation peak of MB appeared at about −0.25 V, strongly demonstrating that D3 could cleave electrode surface-bound H3-Fc to obtain low Fc response and G-MB also could be successfully captured on the electrode surfaces. Therefore, these results noted that the proposed biosensor was reasonable and may provide a new method for Hg^{2+} detection.

Optimization of the Reaction Conditions. In this work, Mg^{2+} not only acted as the cofactor of D1, D2, and D3, but also impacted the capture of G-MB on electrode surface. Thus, investigating the concentration of Mg^{2+} was indispensable for the best performance of the ratiometric electrochemical biosensor. As shown in Figure 3A, the I_{MB}/I_{Fc} value for 0.1 nM Hg^{2+} increased gradually as the Mg^{2+} concentration increased and reached a plateau when the concentration of Mg^{2+} was adjusted to 40 mM. Thus, 40 mM as the optimal of Mg^{2+} concentration was adopted in the subsequent work.

Furthermore, the cleavage reaction of BFDN toward H1 and H2-MB was a key step for the performance of this biosensor, thus the effect of cleavage time (20, 40, 60, 80, and 100 min) of BFDN on the electrode was also studied at 0.1 nM Hg^{2+}. It was apparent that the I_{MB}/I_{Fc} value greatly increased with the extension of cleavage time until 60 min, suggesting that 60 min was adequate for cleavage reaction (Figure 3B).

Moreover, the incubation time of cleavage products of BFDN (D3 and G-MB) on electrode surface would affect the cleavage of D3 toward H3-Fc and the capture of G-MB, causing huge influence to the biosensor. Therefore, we also assessed the incubation time of D3 and G-MB. As shown in Figure 3C, the I_{MB}/I_{Fc} value increased over time and attained the maximum after 80 min. Thus, 80 min was viewed as the optimum incubation time of D3 and G-MB.

Electrochemical Assay of Hg^{2+}. Under optimal experimental conditions, different concentrations of Hg^{2+} were measured to verify the ability of the ratiometric electrochemical biosensor. As presented in Figures 4A and 4B, the electrochemical response of MB increased while the electrochemical response of Fc decreased with the increase of Hg^{2+} concentration. Concomitantly, the calibration curve was also established by using the logarithm of Hg^{2+} concentration as abscissa and the logarithm of the ratio (I_{MB}/I_{Fc}) as ordinate, demonstrating a fine linear relationship between the logarithm of the ratio (I_{MB}/I_{Fc}) and the logarithm of Hg^{2+} concentration ranging from 0.1 pM to 200 nM (Figure 4C). The corresponding linear regression equation was $\lg(I_{MB}/I_{Fc}) = 0.1774 \lg c - 0.1292$ ($r = 0.9933$). In addition, Table 1 depicted that the proposed method here exhibited a wider linear range as well as a lower detection limit down to 23 fM, in comparison to previous methods for Hg^{2+} detection, implying excellent analytical performance of BFDN in the ratiometric electrochemical biosensor.

Selectivity, Stability, and Reproducibility of the Biosensor. To investigate the selectivity of the biosensor, we conducted interference tests to detect various metal ions

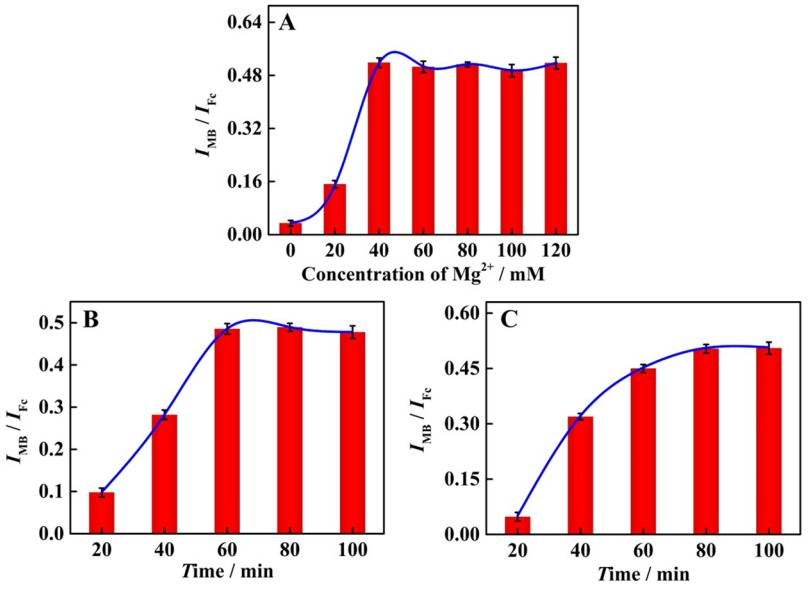

Figure 3. (A) Effect of the concentration of Mg^{2+} on electrode response, (B) Effect of BFDN cleavage time on electrode response, (C) Optimum incubation time of D3 and G-MB. The I_{MB}/I_{Fc} values were obtained with 0.1 nM Hg^{2+}. Error bars: standard deviation (SD), $n = 3$.

DOI: 10.1021/acs.analchem.9b00690
Anal. Chem. 2019, 91, 6127−6133

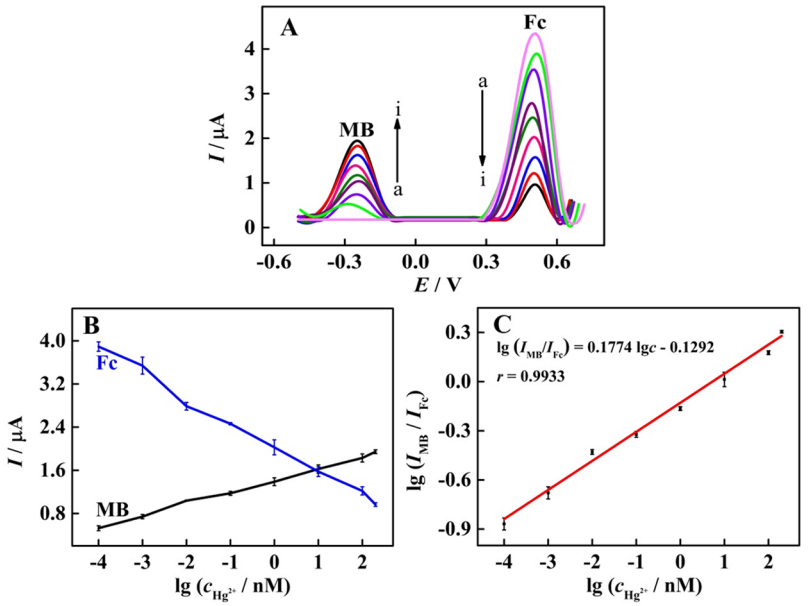

Figure 4. (A) SWV responses of the ratiometric electrochemical biosensor toward different Hg^{2+} concentrations (from curve a to curve i): 0 pM, 0.1 pM, 1 pM, 10 pM, 100 pM, 1 nM, 10 nM, 100 nM, and 200 nM, (B) Dependence of I_{MB} and I_{Fc} on the logarithm of Hg^{2+} concentration, (C) The calibration plot of logarithmic value of I_{MB}/I_{Fc} versus the logarithm of Hg^{2+} concentration. Error bars: SD, n = 3.

Table 1. Comparison of This Work with Other Reports for Hg^{2+} Detection[a]

method	signal amplification strategy	response range	detection limit	ref
visual detection	EASA	1 pM-100 nM	1 pM	38
colorimetric	AuNPs	5 pM-25 nM	1.4 pM	39
SERS	AuNPs decorated silicon nanowire array	1 pM-100 nM	0.73 pM	40
fluorescent	catalytic hairpin assembly	10 pM-100 nM	4.5 pM	41
PEC	CdS quantum dots	5 pM-500 pM	1 pM	42
electrochemical	GQDs	1.0 nM-500 nM	9.8 pM	43
electrochemical	silver nanoparticles	100 pM-10 nM	28 pM	44
electrochemical	EASA	0.1 pM-10 nM	0.042 pM	45
electrochemical	EASA	10 pM-50 nM	1.6 pM	46
electrochemical	BFDN	0.1 pM-200 nM	23 fM	this work

[a]EASA, enzyme-assisted signal amplification; AuNPs, Au nanoparticles; SERS, surface-enhanced Raman scattering; PEC, photoelectrochemical; GQDs, graphene quantum dots.

(Zn^{2+}, Pb^{2+}, Ni^{2+}, Fe^{3+}, Cu^{2+}, Co^{2+}, Cd^{2+}, Ca^{2+}, Ba^{2+}). As illustrated in Figure 5A, whether one type of interfering ion or the mixture of all interfering ions was tested, the I_{MB}/I_{Fc} value was almost negligible, despite the concentration of the interfering ion as high as 10 nM. Inversely, once a small amount of Hg^{2+} (0.1 nM) were mixed with these interfering ions, the I_{MB}/I_{Fc} values increased rapidly and tremendously higher than that in the absence of Hg^{2+}, clearly indicating high selectivity of this fabricated biosensor against other interfering ions. Next, the stability of the biosensor was also monitored by storing the biosensor at 4 °C and measuring intermittently (every 5 days). And the I_{MB}/I_{Fc} value of the biosensor could still keep at 90.3% of its initial value after 20 days, suggesting that the biosensor had great performance in stability (Figure 5B). Moreover, five different batches of the biosensors (interassay) and five biosensors in same batch (intra-assay) for detecting 0.1 nM Hg^{2+} were prepared to explore the reproducibility, which all performed similar I_{MB}/I_{Fc} values and the relative standard deviation (RSD) were 3.5% and 3.0%, respectively, implying acceptable reproducibility of the biosensor (Figure S2).

Practical Application. In order to assess the effectiveness of this ratiometric electrochemical biosensor in practical application, recovery experiments were performed using tap water collected from our laboratory. First, no Hg^{2+} was found in tap water. Then, the tap water samples spiked with Hg^{2+} at five different concentrations of 0.01, 0.1, 1, 10, and 100 nM were tested, obtaining satisfactory recoveries in the range of 91.68% to 108.0% listed in Table 2. Simultaneously, the tap water sample spiked with Hg^{2+} at 10 nM was also tested by inductively coupled plasma mass-spectrometric (ICP-MS) and the obtained concentration was 11.44 nM, which was very close to the result obtained by the ratiometric electrochemical biosensor. Thus, all these testing results indicated potential application of this biosensor in real samples containing Hg^{2+}.

CONCLUSION

In conclusion, by designing the simple BFDN as a powerful tool to trigger two synchronous detection paths, a novel ratiometric electrochemical biosensor was fabricated for sensitive Hg^{2+} detection in this work, showing many laudable features, as follows: First, two synchronous detection paths could be cross-referenced to monitor the entire experimental process, leading to great enhancement of detection reliability and accuracy, compared with the traditional single detection path. Second, the biosensor proposed a novel ratiometric method, effortlessly conquering the troubling deficiency of distance-dependent signal adjustment existed in previous labeled ratiometric electrochemical biosensor. Finally, the

DOI: 10.1021/acs.analchem.9b00690
Anal. Chem. 2019, 91, 6127−6133

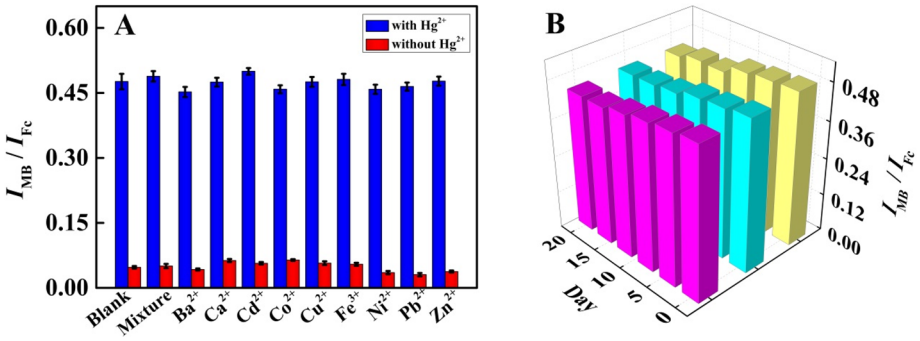

Figure 5. (A) Selectivity of the biosensor for Hg^{2+} (0.1 nM) against other metal ions (each at 10 nM), (B) Stability of the biosensor (0.1 nM Hg^{2+}). Error bars: SD, n = 3.

Table 2. Recovery Experiments of Hg^{2+} in Tap Water Samples

sample	added Hg^{2+} (nM)	found Hg^{2+} (nM)	recovery (%)	relative standar ddeviation, RSD (%)
1	0.01	0.009168	91.68	2.6
2	0.1	0.09773	97.73	7.2
3	1	0.9456	94.56	5.6
4	10	10.80	108.0	4.9
5	100	106.1	106.1	4.1

design of BFDN skillfully combined the advantages of branched DNA nanostructures and DNAzyme, which not only effectively improved the sensitivity and accuracy of Hg^{2+} detection, but also rose up a new path to improve the performances of multifunctional DNA nanomachines by integrating various signal amplification strategies, facilitating the development of DNA nanomachines in the biosensor system.

■ ASSOCIATED CONTENT

Supporting Information

The Supporting Information is available free of charge on the ACS Publications website at DOI: 10.1021/acs.analchem.9b00690.

Reagents, apparatus, polyacrylamide gel electrophoresis, and the reproducibility of the biosensor (Figure S2) (PDF)

■ AUTHOR INFORMATION

Corresponding Authors

*Tel.: +86-23-68252277. Fax: +86-23-68253172. E-mail : yuanruo@swu.edu.cn (R. Yuan).

*Tel.: +86-23-68252277. Fax: +86-23-68253172. E-mail : yqchai@swu.edu.cn (Y. Chai).

ORCID

Ruo Yuan: 0000-0003-3664-6236

Yaqin Chai: 0000-0003-4392-9592

Notes

The authors declare no competing financial interest.

■ ACKNOWLEDGMENTS

This paper was financially supported by the National Natural Science Foundation of China (Nos. 21675129, 21775124, and 21575116) and the Fundamental Research Funds for the Central Universities, China (No. XDJK2018AA003).

■ REFERENCES

(1) Jin, H.; Gui, R. J.; Yu, J. B.; Lv, W.; Wang, Z. H. *Biosens. Bioelectron.* **2017**, *91*, 523−537.

(2) Wu, L.; Ding, F.; Yin, W. M.; Ma, J.; Wang, B. R.; Nie, A.; Han, H. Y. *Anal. Chem.* **2017**, *89*, 7578−7585.

(3) Xiong, E. H.; Zhang, X. H.; Liu, Y. Q.; Zhou, J. W.; Yu, P.; Li, X. Y.; Chen, J. H. *Anal. Chem.* **2015**, *87*, 7291−7296.

(4) Xiong, E. H.; Li, Z. Z.; Zhang, X. H.; Zhou, J. W.; Yan, X. X.; Liu, Y. Q.; Chen, J. H. *Anal. Chem.* **2017**, *89*, 8830−8835.

(5) Zhu, C. X.; Liu, M. Y.; Li, X. Y.; Zhang, X. H.; Chen, J. H. *Chem. Commun.* **2018**, *54*, 10359−10362.

(6) Cui, L.; Lu, M. F.; Li, Y.; Tang, B.; Zhang, C. Y. *Biosens. Bioelectron.* **2018**, *102*, 87−93.

(7) Silva, S. M.; Tavallaie, R.; Goncales, V. R.; Utama, R. H.; Kashi, M. B.; Hibbert, D. B.; Tilley, R. D.; Gooding, J. J. *Langmuir* **2018**, *34*, 1249−1255.

(8) Kekedy-Nagy, L.; Ferapontova, E. E. *J. Phys. Chem. B* **2018**, *122*, 10077−10085.

(9) Lu, N.; Pei, H.; Ge, Z. L.; Simmons, C. R.; Yan, H.; Fan, C. H. *J. Am. Chem. Soc.* **2012**, *134*, 13148−13151.

(10) Zuo, X. L.; Song, S. P.; Zhang, J.; Pan, D.; Wang, L. H.; Fan, C. H. *J. Am. Chem. Soc.* **2007**, *129*, 1042−1043.

(11) Abi, A.; Ferapontova, E. E. *J. Am. Chem. Soc.* **2012**, *134*, 14499−14507.

(12) Monserud, J. H.; Schwartz, D. K. *ACS Nano* **2014**, *8*, 4488−4499.

(13) Farjami, E.; Campos, R.; Ferapontova, E. E. *Langmuir* **2012**, *28*, 16218−16226.

(14) Deng, C. Y.; Pi, X. M.; Qian, P.; Chen, X. Q.; Wu, W. M.; Xiang, J. *Anal. Chem.* **2017**, *89*, 966−973.

(15) Ge, L.; Wang, W. X.; Li, F. *Anal. Chem.* **2017**, *89*, 11560−11567.

(16) Du, Y.; Lim, B. J.; Li, B. L.; Jiang, Y. S.; Sessler, J. L.; Ellington, A. D. *Anal. Chem.* **2014**, *86*, 8010−8016.

(17) Seeman, N. C.; Sleiman, H. F. *Nat. Rev. Mater.* **2017**, *3*, 17068.

(18) Bui, H.; Shah, S.; Mokhtar, R.; Song, T. Q.; Garg, S.; Reif, J. *ACS Nano* **2018**, *12*, 1146−1155.

(19) Zhang, P.; Jiang, J.; Yuan, R.; Zhuo, Y.; Chai, Y. Q. *J. Am. Chem. Soc.* **2018**, *140*, 9361−9364.

(20) Liu, Q.; Ge, Z. L.; Mao, X. H.; Zhou, G. B.; Zuo, X. L.; Shen, J. W.; Shi, J. Y.; Li, J.; Wang, L. H.; Chen, X. Q.; Fan, C. H. *Angew. Chem., Int. Ed.* **2018**, *57*, 7131−7135.

(21) Zhang, C.; Li, X.; Tian, C.; Yu, G. M.; Li, Y. L.; Jiang, W.; Mao, C. D. *ACS Nano* **2014**, *8*, 1130−1135.

(22) Jung, C.; Allen, P. B.; Ellington, A. D. *Nat. Nanotechnol.* **2016**, *11*, 157−163.

(23) Li, C.; Hu, X. L.; Lu, J. Y.; Mao, X. X.; Xiang, Y.; Shu, Y. Q.; Li, G. X. *Chem. Sci.* **2018**, *9*, 979−984.

(24) Lin, M. H.; Wang, J. J.; Zhou, G. B.; Wang, J. B.; Wu, N.; Lu, J. X.; Gao, J. M.; Chen, X. Q.; Shi, J. Y.; Zuo, X. L.; Fan, C. H. *Angew. Chem.* **2015**, *127*, 2179−2183.

DOI: 10.1021/acs.analchem.9b00690
Anal. Chem. 2019, 91, 6127−6133

(25) Birkholz, O.; Burns, J. R.; Richter, C. P.; Psathaki, O. E.; Howorka, S.; Piehler, J. *Nat. Commun.* **2018**, *9*, 1521.
(26) Wu, C. C.; Han, D.; Chen, T.; Peng, L.; Zhu, G. Z.; You, M. X.; Qiu, L. P.; Sefah, K.; Zhang, X. B.; Tan, W. H. *J. Am. Chem. Soc.* **2013**, *135*, 18644−18650.
(27) Mo, A. H.; Landon, P. B.; Meckes, B.; Yang, M. M.; Glinsky, G. V.; Lal, R. *Nanoscale* **2014**, *6*, 1462−1466.
(28) Zhang, L. B.; Guo, S. J.; Zhu, J. B.; Zhou, Z. X.; Li, T.; Li, J.; Dong, S. J.; Wang, E. K. *Anal. Chem.* **2015**, *87*, 11295−11300.
(29) Yang, L.; Yao, C.; Li, F.; Dong, Y. H.; Zhang, Z. K.; Yang, D. Y. *Small* **2018**, *14*, 1800185.
(30) Liu, D.; Chen, G.; Akhter, U.; Cronin, T. M.; Weizmann, Y. *Nat. Chem.* **2016**, *8*, 907.
(31) He, M. Q.; Wang, K.; Wang, W. J.; Yu, Y. L.; Wang, J. H. *Anal. Chem.* **2017**, *89*, 9292−9298.
(32) Yan, T. T.; Zhu, L. Y.; Ju, H. X.; Lei, J. P. *Anal. Chem.* **2018**, *90*, 14493−14499.
(33) Wang, S.; Cazelles, R.; Liao, W.; Vazquez-Gonzalez, M.; Zoabi, A.; Abu-Reziq, R.; Willner, I. *Nano Lett.* **2017**, *17*, 2043−2048.
(34) Chen, W. H.; Yu, X.; Cecconello, A.; Sohn, Y. S.; Nechushtai, R.; Willner, I. *Chem. Sci.* **2017**, *8*, 5769−5780.
(35) Wei, Q. M.; Huang, J.; Li, J.; Wang, J. L.; Yang, X. H.; Liu, J. B.; Wang, K. M. *Chem. Sci.* **2018**, *9*, 7802−7808.
(36) Chen, F.; Bai, M.; Cao, K.; Zhao, Y.; Cao, X. W.; Wei, J.; Wu, N.; Li, J.; Wang, L. H.; Fan, C. H.; Zhao, Y. X. *ACS Nano* **2017**, *11*, 11908−11914.
(37) Wu, N.; Willner, I. *Nano Lett.* **2016**, *16*, 2867−2872.
(38) Chen, J. H.; Zhou, S. G.; Wen, J. L. *Anal. Chem.* **2014**, *86*, 3108−3114.
(39) Liu, X. J.; Wu, Z. J.; Zhang, Q. Q.; Zhao, W. F.; Zong, C. H.; Gai, H. W. *Anal. Chem.* **2016**, *88*, 2119−2124.
(40) Sun, B.; Jiang, X. X.; Wang, H. Y.; Song, B.; Zhu, Y.; Wang, H.; Su, Y. Y.; He, Y. *Anal. Chem.* **2015**, *87*, 1250−1256.
(41) Li, X.; Xie, J. Q.; Jiang, B. Y.; Yuan, R.; Xiang, Y. *ACS Appl. Mater. Interfaces* **2017**, *9*, 5733−5738.
(42) Ma, Z. Y.; Pan, J. B.; Lu, C. Y.; Zhao, W. W.; Xu, J. J.; Chen, H. Y. *Chem. Commun.* **2014**, *50*, 12088−12090.
(43) Lu, L. L.; Zhou, L.; Chen, J.; Yan, F.; Liu, J. Y.; Dong, X. P.; Xi, F. N.; Chen, P. *ACS Nano* **2018**, *12*, 12673−12681.
(44) Suherman, A. L.; Ngamchuea, K.; Tanner, E. E. L.; Sokolov, S. V.; Holter, J.; Young, N. P.; Compton, R. G. *Anal. Chem.* **2017**, *89*, 7166−7173.
(45) Cai, W.; Xie, S. B.; Zhang, J.; Tang, D. Y.; Tang, Y. *Biosens. Bioelectron.* **2017**, *98*, 466−472.
(46) Hong, M. Q.; Wang, M. Y.; Wang, J.; Xu, X. Q.; Lin, Z. Y. *Biosens. Bioelectron.* **2017**, *94*, 19−23.

DOI: 10.1021/acs.analchem.9b00690
Anal. Chem. 2019, 91, 6127−6133